Neutral and charged biexciton-exciton cascade in near-telecom-wavelength quantum dots

Jan Kettler,[*,‡] Matthias Paul, Fabian Olbrich, Katharina Zeuner,[†] Michael Jetter, and Peter Michler
Institut für Halbleiteroptik und Funktionelle Grenzflächen, Center for Integrated Quantum Science and Technology (IQ^{ST}) and SCoPE, University of Stuttgart, Allmandring 3, 70569 Stuttgart, Germany

Matthias Florian, Christian Carmesin, and Frank Jahnke
Institute of Theoretical Physics, University of Bremen, P.O. Box 330440, 28334 Bremen, Germany
(Received 21 April 2016; revised manuscript received 30 May 2016; published 8 July 2016)

We investigate the cascaded emission of photons from low-density InGaAs/GaAs quantum dots grown by metal-organic vapor-phase epitaxy that are intentionally redshifted toward telecommunication wavelengths. We observe multiple radiative cascades within a single quantum dot and attribute these to neutral and charged excited configurations. The corresponding transitions are identified by combining microphotoluminescence and photon correlation measurements. Full-configuration interaction calculations further support the identification of the emission lines and provide additional information about the confinement of electron and hole wave functions. We apply a Monte Carlo simulation to estimate the effective spin scattering rates between excited triplet and singlet ground states of the negatively charged trion. These spin-flip processes directly affect the observed radiative cascade.

DOI: 10.1103/PhysRevB.94.045303

I. INTRODUCTION

Among other systems, semiconductor quantum dots (QDs) are sources of single photons that can potentially contribute to future long-distance quantum communication protocols. One of the requirements for these sources is the creation of entangled photons, which has been shown for QDs with polarization-entangled [1–3] as well as time-bin-entangled photon pairs [4]. Both of these entanglement schemes rely on the existence of a biexciton-exciton cascade. A second requirement is the ability to effectively distribute photons over long distances, which, in the case of a fiber-based quantum network, does greatly benefit from photons within the telecommunication wavelength bands around 1.55 μm (C-band) where standard silica fibers show the lowest absorption losses, and, at 1.31 μm (O-band) where dispersion is minimal [5]. Further, on-chip silicon quantum photonics may strongly profit from semiconductor single-photon sources above 1.1 μm [6]. Yet, the most elaborate results employing QDs as sources of nonclassical light have been achieved in the InAs material system at wavelengths below 1 μm with only a few studies addressing the single-dot properties of redshifted and thus typically larger QDs, suitable for quantum light sources [7–17].

In this work, we analyze the emission properties of InGaAs/GaAs QDs grown by metal-organic vapor-phase epitaxy (MOVPE) which have been intentionally modified to provide redshifted emission at wavelengths above 1.1 μm. The photoluminescence spectrum contains a series of emission lines, which are attributed to transitions between various multi-exciton states. A central goal of this work is to identify the contributing configurations and the underlying carrier dynamics. From our experiments, we obtain information about the energetic position of the emission lines, their excitation power dependence, the temporal correlation of cascaded photon emission from different lines, as well as polarization-dependent shifts of the emission lines with fine-structure splitting (FSS). On the theory side, we use full configuration interaction (FCI) calculations [18] to identify the energetic position of various multi-exciton states in terms of a given confinement potential. Furthermore, the role of spin scattering from the excited trion triplet to the singlet ground states is analyzed using a Monte Carlo simulation.

II. EXPERIMENT

The deposition of low-density InAs QDs on a GaAs substrate typically leads to ground-state emission wavelengths below 1 μm. Moreover, due to the efficiency of standard silicon detectors, InAs QDs are often treated with further techniques, such as partial capping and annealing, to achieve an additional blueshift. The availability of highly efficient detectors at longer wavelengths [19] now supports the desire to achieve the opposite effect for low-density InAs QDs in order to benefit from the telecommunication windows. The growth of the QDs under investigation has been adapted in two ways to support an efficient redshift of the emission wavelength: First, InGaAs has been deposited instead of pure InAs QD material. The reduced lattice mismatch leads to the growth of less strained and larger coherent QD structures, which in the case of an appropriate composition is sufficient to overcompensate for the effect of a chemically increased InGaAs band gap. Second, instead of a direct GaAs capping, a thin InGaAs layer has been deposited on top of the QDs that helps to maintain, or even raise, the QD size and In concentration upon GaAs overgrowth [20] and simultaneously reduces the strain induced by the GaAs cap (strain-reducing layer, SRL). In order to increase the photoluminescence collection efficiency, a 10-pair distributed Bragg reflector (DBR) is included between the GaAs substrate and QD layer forming a weak λ cavity of $\approx$365 nm. A sketch

[*]j.kettler@ihfg.uni-stuttgart.de
[†]Present address: Department of Applied Physics, Royal Institute of Technology (KTH), 10691 Stockholm, Sweden.
[‡]www.ihfg.uni-stuttgart.de

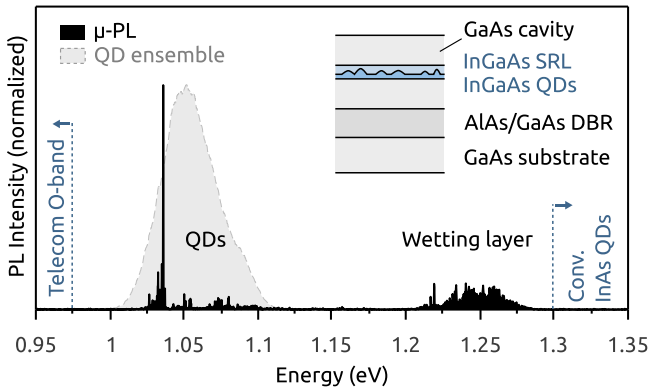

FIG. 1. μ-PL emission (black) between 920 nm (1.35 eV) and 1300 nm (0.95 eV). The InGaAs QD ensemble emission (gray) has been lowered by ≈250 meV with respect to conventional InAs QDs. Inset: Layer structure of the sample.

of the layer structure of the sample is displayed in the inset of Fig. 1.

The measurements are carried out in a standard microphotoluminescence (μ-PL) setup at a temperature of approximately 4 K. Photoexcited carriers are generated with an off-resonant laser above the GaAs band gap. Emission from the QDs is collected with an infra-red (IR) microscope objective (numerical aperture 0.6), coupled to a single-mode fiber and spectrally analyzed by a 0.5 m spectrograph equipped with an InGaAs charge-coupled device (CCD). Temporal analysis is achieved using superconducting nanowire single-photon detectors with a quantum efficiency of 15% and an overall timing resolution of ≈150 ps (including coincidence electronics).

III. RESULTS AND DISCUSSION

The decrease in the emission energy of the investigated QDs reaches approximately 250 meV with respect to their conventional InAs counterparts, as displayed in Fig. 1. Choosing appropriate growth parameters for the QDs and InGaAs layer, a low lateral density can be obtained over the spectral range from 900 nm up to 1300 nm [21,22]. The sample under study exhibits a lateral density of $\approx 2\times10^8$ cm^{-2} that allows single-dot spectroscopy without further isolation techniques. For the main transition lines observed in the nonresonantly excited QDs, we typically find linewidths below 80 μeV, lifetimes of ≈1 ns, and a mean FSS of ≈50 μeV resembling values obtained from standard InAs QDs.

Owing to the above-band excitation, several transitions can be found that originate from multiple neutral and charged configurations of the same emitter. We often observe more than one pair of transitions with a FSS apparent among the weaker emission lines while the main line is generally not split. A μ-PL spectrum of a single QD with the most frequently observed emission pattern and assigned single- and biexcitonic transitions is plotted in Fig. 2(a). The assignment of the spectral lines follows a combination of excitation power and polarization-resolved μ-PL measurements, as displayed in Figs. 2(b)–2(d). Due to the discussion below, we assume, in the case of occupation by an unequal number of electrons

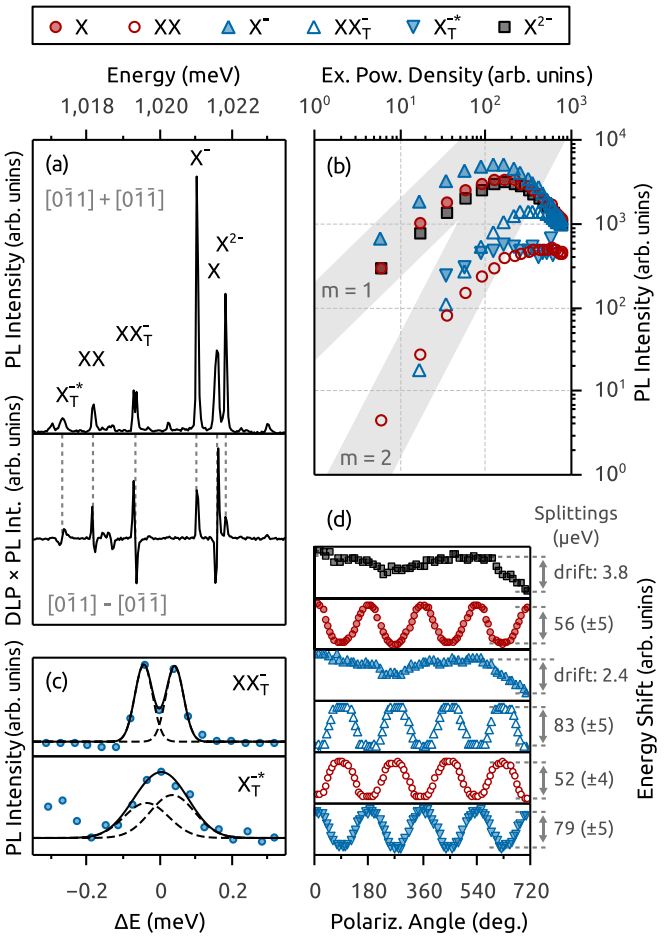

FIG. 2. μ-PL indications of cascaded emission. (a) Assignment of the main optical transitions deduced from (b)–(d). Lower part: PL intensity multiplied by the degree of linear polarization (DLP). (b) Linear ($m = 1$) and quadratic ($m = 2$) dependencies of the μ-PL intensity on the excitation power density. (c) Magnification of the negative biexciton and excited trion triplet transition lines. (d) Polarization-dependent shift of the emission lines due to the underlying FSS. Equally split pairs with a converse dependency indicate a direct radiative cascade.

and holes, to predominantly observe the negatively charged configuration.

A first classification into single- and multi-excitonic states is found from the dependency of the PL recombination rates on the excitation power density [Fig. 2(b)]. Since below saturation, the probability to capture a distinct number of electron-hole (e-h) pairs follows Poisson statistics [23], this yields linear and quadratic dependencies for the occupation of exciton ($|X\rangle$) and biexciton ($|XX\rangle$), respectively. For absent single-charge escape channels, generally this also applies to charged exciton ($|X^-\rangle$, $|X^{2-}\rangle$) and biexciton ($|XX^-\rangle$) states. The assignment to neutral and charged configurations is obtained considering the underlying FSS. Four of the six brightest transition lines exhibit a polarization-dependent substructure [Fig. 2(a), lower part]. As these splittings are often close to, or below, the resolution limit of the spectrometer [Fig. 2(c)], our analysis exploits the subtle shift of the combined emission line that can be observed by suppressing a distinct fine-structure

component by polarization-selective filtering [24]. In this way the minimal observable splitting is predominantly limited by the signal-to-noise ratio. The polarization-dependent shifts and the extracted FSS are shown in Fig. 2(d). The main emission line is identified as emission from the negative trion ground state, where two electrons form a spin singlet configuration that cancels the anisotropic e-h exchange interaction. The remaining drift is a good estimation for the lower limit of detectable splittings. Further, exciton and biexciton transitions exhibit splittings of the same size ($\approx$50 μeV) with a converse polarization relation as expected from both decay paths of the neutral biexciton-exciton cascade [Fig. 3(a)].

For the charged biexciton, the situation is more intricate, as the subsequent cascade naturally includes additional decay channels due to the involved p-shell carrier [Figs. 3(b) and 3(c)]. Following the recombination of an s-shell e-h pair, an excited trion state ($|X^{-*}\rangle$) is populated where both electrons are distributed over s- and p-shells. Here, two unpaired electron spins and a single hole spin yield eight possible configurations that are split into four degenerate doublets by the electron-electron (e-e) and e-h exchange interaction [25,26]. Figure 4(c) shows a pictographic representation of the spin parts of the wave functions. For simplicity, only one branch of each degenerate doublet is displayed. The strongest contribution to the excited trion FSS follows from the (isotropic) e-e exchange interaction, introducing a splitting between singlet and triplet spin configurations on the order of the Coulomb energy between two electrons. A weaker contribution, mainly from the isotropic e-h exchange interaction, results in the splitting of the triplet states on the order of the energy difference between dark and bright neutral excitons. The anisotropic part of the e-h exchange interaction causes mixing of the triplet states $|T_0\rangle$ ($J_z = \pm 3/2$) and $|T_1\rangle$ ($J_z = \mp 1/2$) that, contrary to the neutral exciton case, leaves the degeneracy of the doublets unaffected. However, it results in orthogonal elliptically polarized optical

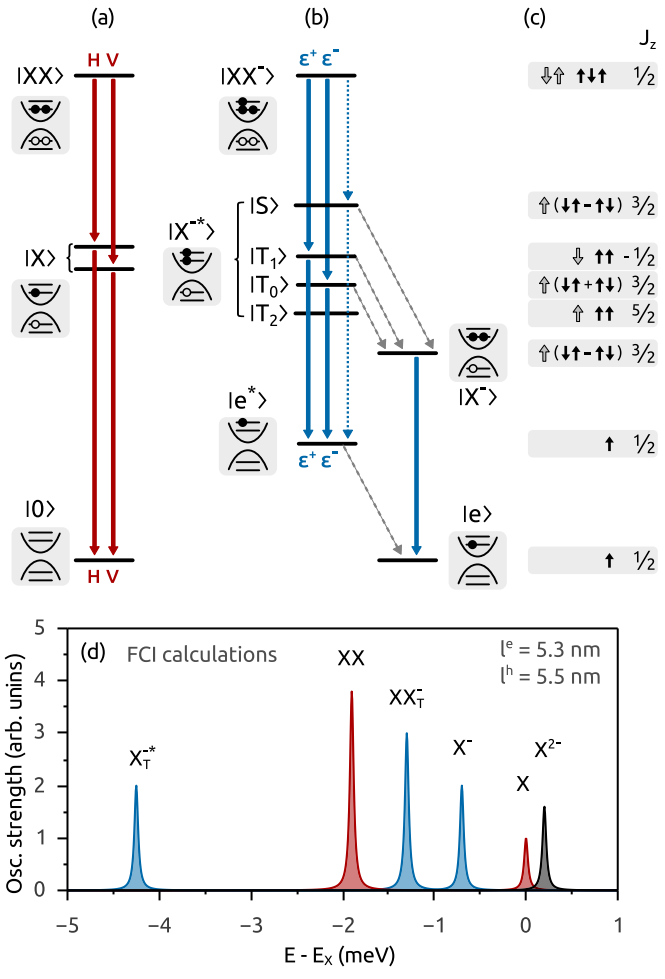

FIG. 3. Level structures of (a) neutral (red) and (b) charged (blue) radiative cascades (not to scale) and polarization of the direct cascades; also shown are pictographic representations of the populated QD shells. (c) Spin part of the wave function of the negatively charged states. Electrons: black; holes: gray. Spin configurations are given for only one of two Kramers-degenerate branches. (d) Energetic ordering of the transition energies obtained by FCI calculations.

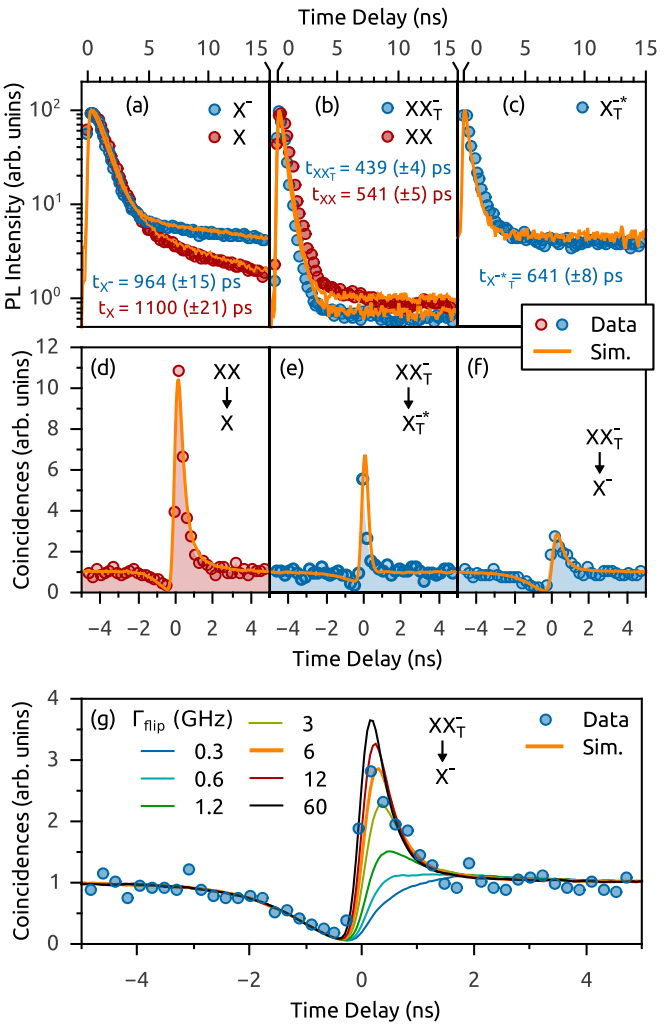

FIG. 4. (a)–(c) Time-resolved μ-PL transients of the cascade related transitions. (d)–(f) Intensity cross-correlation measurements of three pairs of emission lines showing cascaded photon emission. (g) Monte Carlo simulation of the indirect negatively charged cascade under variation of the average scattering rate between excited trion triplet and singlet ground state. Simulations for the parameter set with the best agreement are plotted in (a)–(f).

transitions [26,27]. The mixing of the lowest triplet state $|T_2\rangle$ ($J_z = \pm 5/2$) on the order of the neutral dark exciton splitting is typically much weaker [28], retaining negligible optical transitions. Hence the pair of lines with a converse FSS of $\approx$80 μeV in Fig. 2(d) is attributed to the transitions from charged biexciton to the excited trion triplet $|XX^-\rangle \rightarrow |T_{0,1}\rangle$ (XX_T^-) and further to the excited (p-shell) electron $|T_{0,1}\rangle \rightarrow |e^*\rangle$ (X_T^{-*}). We observe a strong degree of linear polarization (DLP) for both transitions (XX_T^-: > 0.74, X_T^{-*}: > 0.92), indicating substantial contribution from the anisotropic part of the exchange interaction. It should be noted that also the charged biexciton transition to the excited singlet trion ($|XX^-\rangle \rightarrow |S\rangle$) should be observable as an unpolarized emission line, substantially broadened due to the subsequent fast relaxation of the target state. However, insufficient signal strengths of the remaining transitions limit further investigations.

With the assignment found above, we compare the energetic ordering of the transitions to the emission spectrum obtained through effective mass FCI calculations [18,29–32], assuming the solution of a quantum well along the QD growth axis and a two-dimensional harmonic oscillator for the lateral confinement. We further assume rotational symmetry around the QD axis and spin-degenerate single-particle states. As far as more information about the morphology is available, atomistic calculation can be used [20,28,33]. Choosing typical parameters for the InGaAs material system [18], the electron and hole envelope functions are varied to achieve the best agreement with the experimental spectrum. As observed in earlier works [34], the ordering of the ground-state trion, charged biexciton, and excited trion triplet follows a general rule, as the sp-exchange energy typically overcomes the negative biexciton binding energy. However, the energetic order including the neutral exciton and biexciton can only be obtained assuming similar envelopes for electrons and holes. Figure 3(d) shows the calculated emission spectrum when considering the confinement of a complete s- and p-shell, and an extension of the wave-function envelopes of $l^e = 5.3$ nm and $l^h = 5.5$ nm for electrons and holes, respectively. Obviously, this implies a more homogeneous situation for electron and hole confinement than reported for QDs emitting in a similar wavelength range [35,36]. For the model used, a splitting between s- and p-shell excitons of 61 meV is obtained in good agreement with the experimental observations [20]. The calculations further support the assignment of the transition above the neutral exciton to the main component [37] of the double negatively charged trion [cf. Fig. 2(a)], as no reasonable parameters can be found that suggest, e.g., the assignment to a positive ground-state trion and simultaneously maintain the observed ordering of neutral and negatively charged transitions. Also, the additional confinement of a QD d-shell and resulting renormalization effects would lead to a further redshift of the multi-exciton complexes with respect to the ground-state exciton, which is even more pronounced if further shells are included [38]. More details about the FCI calculations can be found in the Supplemental Material [39].

We confirm the cascaded emission of photons by analyzing the time-resolved μ-PL [Figs. 4(a)–4(c)] and intensity cross-correlation functions [Figs. 4(d)–4(f)] of the transitions discussed above. PL time traces show that by means of two decay channels, the biexcitonic decay rates [Fig. 4(b)] approximately double those of the single-exciton states [Fig. 4(a)], as expected for the strong confinement regime [40]. Despite a weaker oscillator strength, the excited trion triplet lifetime is shorter than the ground-state trion due to the additional relaxation channel. Correlated photon emission is found for three pairs of the observed transitions: In addition to the neutral biexciton-exciton cascade [Fig. 4(d)] and the direct negatively charged biexciton-exciton cascade [Fig. 4(e)], we find cascaded emission from the charged biexciton followed by the ground-state trion [4(f)]. For that, the excited trion triplet is required to undergo a longitudinal (case of $|T_1\rangle$) or transversal (case of $|T_0\rangle$) spin flip, during the relaxation to the ground-state trion. A dominating longitudinal spin flip has been reported for negatively charged states [41] while the opposite has been reported for positively charged trions [42,43]. In our case, a strong linear polarization and similar amplitudes of charged biexciton and excited triplet components [cf. Figs. 2(c) and 2(d)] suggest a substantial mixing of $|T_1\rangle$ and $|T_0\rangle$, rendering this classification invalid.

To estimate the relaxation rates from the trion triplet states to the singlet ground state, we adapt a Monte Carlo random population model [23] to approximately reproduce PL transients and coincidence measurements of the QD under nonresonant excitation. For this we consider a QD with spin-resolved s- and p-shell states, a charge-carrier trap for electrons and holes, and a carrier reservoir. In a first step, we fix several system parameters to the data extracted from the intensity transients and μ-PL spectrum, i.e., QD charging probability (X–X^- intensity relation), carrier capture times (transient rise times), decay times (transient fast decay), trap population and relaxation times (transient slow decay), and excitation rate (PL intensity with respect to saturation). Considering the setup's timing resolution and background contribution, we adapt the average scattering rate from the excited trion triplet to the singlet ground state to the best agreement with the experimental data sets [cf. Figs. 4(a)–4(f)]. We attribute the slight overestimation of the bunching peak of the XX_T^-–X_T^{-*} cascade to the low signal strength of the X_T^{-*} transition, which is most critically affected by possible contribution of other (weak) transition lines. A variation of the spin scattering rate predominantly affects the bunching signature of the indirect XX_T^-–X^- cascade, suggesting a value of $\approx$6 GHz [Fig. 4(g)], which matches the order of magnitude reported in Refs. [41–43].

IV. SUMMARY

In conclusion, we demonstrated the emission of cascaded photons from neutral and charged configurations in long-wavelength emitting InGaAs QDs. The assignment of the transitions and the energetic order of the observed direct and indirect cascades suggests a similar extent of electron and hole wave function. In contrast to studies from standard InAs QDs, the linear polarization of charged biexciton and excited trion transitions (DLP > 0.74) implies a substantial mixing of the trion triplet states. Yet, we estimate a comparable contribution of the spin scattering relaxation of the excited trion triplet state to the singlet ground state ($\approx$6 GHz) as observed in conventional InAs QDs. The neutral biexciton-exciton cascade at telecom wavelength is of high interest, as it

can be exploited to produce polarization or time-bin-entangled photon pairs. Insight into the dynamics of multi-exciton configurations obtained by correlating the emission of charged QD states may be beneficial for experiments targeting the interconnection of single-carrier spins with telecommunication photons.

ACKNOWLEDGMENTS

The authors gratefully acknowledge funding by the Deutsche Forschungsgemeinschaft (JA 619/13-1) and the Federal Ministry of Education and Research (BMBF), in particular for the project Q.com-H (16KIS0115 and 16KIS0111).

[1] N. Akopian, N. H. Lindner, E. Poem, Y. Berlatzky, J. Avron, D. Gershoni, B. D. Gerardot, and P. M. Petroff, Phys. Rev. Lett. **96**, 130501 (2006).
[2] R. M. Stevenson, R. J. Young, P. Atkinson, K. Cooper, D. A. Ritchie, and A. J. Shields, Nature **439**, 179 (2006).
[3] R. Hafenbrak, S. M. Ulrich, P. Michler, L. Wang, A. Rastelli, and O. G. Schmidt, New J. Phys. **9**, 315 (2007).
[4] H. Jayakumar, A. Predojević, T. Kauten, T. Huber, G. S. Solomon, and G. Weihs, Nat. Commun. **5**, 4251 (2014).
[5] G. P. Agrawal, *Fiber-optic Communication Systems*, 4th ed. (Wiley, New York, 2010).
[6] E. Murray, D. J. P. Ellis, T. Meany, F. F. Floether, J. P. Lee, J. P. Griffiths, G. A. C. Jones, I. Farrer, D. A. Ritchie, A. J. Bennett, and A. J. Shields, Appl. Phys. Lett. **107**, 171108 (2015).
[7] M. B. Ward, O. Z. Karimov, D. C. Unitt, Z. L. Yuan, P. See, D. G. Gevaux, A. J. Shields, P. Atkinson, and D. A. Ritchie, Appl. Phys. Lett. **86**, 201111 (2005).
[8] C. Zinoni, B. Alloing, C. Monat, V. Zwiller, L. H. Li, A. Fiore, L. Lunghi, A. Gerardino, H. de Riedmatten, H. Zbinden, and N. Gisin, Appl. Phys. Lett. **88**, 131102 (2006).
[9] D. Dalacu, M. Reimer, S. Fréderick, D. Kim, J. Lapointe, P. Poole, G. Aers, R. Williams, W. Ross McKinnon, M. Korkusinski, and P. Hawrylak, Laser Photon. Rev. **4**, 283 (2009).
[10] D. Dalacu, K. Mnaymneh, V. Sazonova, P. J. Poole, G. C. Aers, J. Lapointe, R. Cheriton, A. J. SpringThorpe, and R. Williams, Phys. Rev. B **82**, 033301 (2010).
[11] T. Miyazawa, T. Kodera, T. Nakaoka, K. Watanabe, N. Kumagai, N. Yokoyama, and Y. Arakawa, Appl. Phys. Express **3**, 064401 (2010).
[12] M. T. Rakher, L. Ma, O. Slattery, X. Tang, and K. Srinivasan, Nat. Photon. **4**, 786 (2010).
[13] M. D. Birowosuto, H. Sumikura, S. Matsuo, H. Taniyama, P. J. van Veldhoven, R. Nötzel, and M. Notomi, Sci. Rep. **2**, 321 (2012).
[14] M. Benyoucef, M. Yacob, J. P. Reithmaier, J. Kettler, and P. Michler, Appl. Phys. Lett. **103**, 162101 (2013).
[15] M. Ward, M. Dean, R. Stevenson, A. Bennett, D. Ellis, K. Cooper, I. Farrer, C. Nicoll, D. Ritchie, and A. Shields, Nat. Commun. **5**, 3316 (2014).
[16] K. Takemoto, Y. Nambu, T. Miyazawa, Y. Sakuma, T. Yamamoto, S. Yorozu, and Y. Arakawa, Sci. Rep. **5**, 14383 (2015).
[17] J.-H. Kim, T. Cai, C. J. K. Richardson, R. P. Leavitt, and E. Waks, Optica **3**, 577 (2016).
[18] N. Baer, P. Gartner, and F. Jahnke, Eur. Phys. J. B **42**, 231 (2004).
[19] F. Marsili, V. B. Verma, J. A. Stern, S. Harrington, A. E. Lita, T. Gerrits, I. Vayshenker, B. Baek, M. D. Shaw, R. P. Mirin, and S. W. Nam, Nat. Photon. **7**, 210 (2013).
[20] E. Goldmann, M. Paul, F. F. Krause, K. Müller, J. Kettler, T. Mehrtens, A. Rosenauer, M. Jetter, P. Michler, and F. Jahnke, Appl. Phys. Lett. **105**, 152102 (2014).
[21] M. Paul, J. Kettler, K. Zeuner, C. Clausen, M. Jetter, and P. Michler, Appl. Phys. Lett. **106**, 122105 (2015).
[22] J. Kettler, M. Paul, F. Olbrich, K. Zeuner, M. Jetter, and P. Michler, Appl. Phys. B **122**, 48 (2016).
[23] M. Grundmann and D. Bimberg, Phys. Rev. B **55**, 9740 (1997).
[24] K. Kowalik, O. Krebs, A. Lemaitre, S. Laurent, P. Senellart, P. Voisin, and J. A. Gaj, Appl. Phys. Lett. **86**, 041907 (2005).
[25] I. A. Akimov, A. Hundt, T. Flissikowski, and F. Henneberger, Appl. Phys. Lett. **81**, 4730 (2002).
[26] K. V. Kavokin, Phys. Status Solidi A **195**, 592 (2003).
[27] I. A. Akimov, K. V. Kavokin, A. Hundt, and F. Henneberger, Phys. Rev. B **71**, 075326 (2005).
[28] G. Bester, S. Nair, and A. Zunger, Phys. Rev. B **67**, 161306 (2003).
[29] A. Barenco and M. A. Dupertuis, Phys. Rev. B **52**, 2766 (1995).
[30] E. Dekel, D. Gershoni, E. Ehrenfreund, D. Spektor, J. M. Garcia, and P. M. Petroff, Phys. Rev. Lett. **80**, 4991 (1998).
[31] P. Hawrylak, Phys. Rev. B **60**, 5597 (1999).
[32] M. Braskén, M. Lindberg, D. Sundholm, and J. Olsen, Phys. Rev. B **64**, 035312 (2001).
[33] M. Zieliński, M. Korkusiński, and P. Hawrylak, Phys. Rev. B **81**, 085301 (2010).
[34] S. M. Ulrich, M. Benyoucef, P. Michler, N. Baer, P. Gartner, F. Jahnke, M. Schwab, H. Kurtze, M. Bayer, S. Fafard, Z. Wasilewski, and A. Forchel, Phys. Rev. B **71**, 235328 (2005).
[35] N. I. Cade, H. Gotoh, H. Kamada, H. Nakano, and H. Okamoto, Phys. Rev. B **73**, 115322 (2006).
[36] L. Sapienza, R. Al-Khuzheyri, A. Dada, A. Griffiths, E. Clarke, and B. D. Gerardot, Phys. Rev. B **93**, 155301 (2016).
[37] M. Ediger, G. Bester, B. D. Gerardot, A. Badolato, P. M. Petroff, K. Karrai, A. Zunger, and R. J. Warburton, Phys. Rev. Lett. **98**, 036808 (2007).
[38] K. Hinzer, P. Hawrylak, M. Korkusinski, S. Fafard, M. Bayer, O. Stern, A. Gorbunov, and A. Forchel, Phys. Rev. B **63**, 075314 (2001).
[39] See Supplemental Material at http://link.aps.org/supplemental/10.1103/PhysRevB.94.045303 for further details about the FCI calculations.
[40] M. Wimmer, S. V. Nair, and J. Shumway, Phys. Rev. B **73**, 165305 (2006).
[41] Y. Benny, R. Presman, Y. Kodriano, E. Poem, D. Gershoni, T. A. Truong, and P. M. Petroff, Phys. Rev. B **89**, 035316 (2014).
[42] E. Poem, Y. Kodriano, C. Tradonsky, B. D. Gerardot, P. M. Petroff, and D. Gershoni, Phys. Rev. B **81**, 085306 (2010).
[43] Y. Igarashi, M. Shirane, Y. Ota, M. Nomura, N. Kumagai, S. Ohkouchi, A. Kirihara, S. Ishida, S. Iwamoto, S. Yorozu, and Y. Arakawa, Phys. Rev. B **81**, 245304 (2010).